Microchimica Acta (2020) 187: 546
https://doi.org/10.1007/s00604-020-04531-0

ORIGINAL PAPER

Au-Co nanoparticles-embedded N-doped carbon nanotube hollow polyhedron modified electrode for electrochemical determination of quercetin

Guiling Luo[1] · Ying Deng[1] · Lin Zhu[1] · Juan Liu[2] · Bingxue Zhang[1] · Yan Zhang[1] · Wei Sun[1] · Guangjiu Li[2]

Received: 4 March 2020 / Accepted: 22 August 2020 / Published online: 4 September 2020

Abstract

A core-shell ZIF-8@ZIF-67 was synthesized and pyrolyzed to get a Co nanoparticles-embedded N-doped carbon nanotube hollow polyhedron (Co@NCNHP). Then Au nanoparticles were formed on the surface and core of Co@NCNHP to obtain an Au-Co bimetal decorated NCNHP (Au-Co@NCNHP). The resultant nanocomposite was characterized by various methods including transmission electron microscopy, scanning electron microscopy, X-ray diffraction, X-ray photoelectron spectroscopy and Fourier transform infrared spectroscopy. The Au-Co@NCNHP-based electrochemical sensor displayed an obviously high electrocatalytic response to the oxidation of quercetin, which was attributed to the synergistic effects of Au-Co bimetal nanoparticles and N-doped carbon nanotube with hollow polyhedron. Under the optimal conditions, the oxidation peak currents exhibited a wide linear dynamic range for quercetin concentration from 0.050 to 35.00 μmol/L, and the detection limit was 0.023 ± 0.002 μmol/L (S/N = 3). The analytical applications of the proposed electrochemical sensor were checked by determining the content of quercetin in medical and onion samples with satisfactory results.

Keywords Core-shell ZIF-8@ZIF-67 · Au-Co bimetal nanoparticles · N-doped carbon nanotube · Hollow polyhedron · Quercetin · Electroanalytical Chemistry

Introduction

Quercetin (3,3′,4′,5,7-penta hydroxyl flavones, QR) is widely present in food of plant origin (such as onions, apples, and tea), which has diverse biological activities such as antitumor activity, cardiovascular protection, antioxidant cataract prevention, and anticancer [1]. Because biological functions are very advantageous for human's health, sensitive determination of QR is very crucial, especially in natural pharmaceutical chemistry, biochemistry, and clinical medicine. Compared with other analytical methods such as high-performance liquid chromatography (HPLC), fluorescence, and spectrophotometry for quantification of QR, electrochemical methods provide more advantages with low/nontoxic sensing nanomaterials, easy preparation procedure, and selective/sensitive analytical results [2–6]. For instance, Zhang et al. [7] developed a sensor for QR determination based on MIL-101 (Cr)/MoS_2–modified glassy carbon electrode (GCE) with molecularly imprinted polymer. Sun et al. manufactured polypyrrole film based molecularly imprinted polymer with incorporated graphene oxide modified GCE for QR determination [8]. Niu et al. used three-dimensional reduced graphene oxide aerogel–modified carbon ionic liquid electrode for QR analysis [9].

As a significant subset of metal-organic frameworks (MOFs), zeolitic imidazolate frameworks (ZIFs) are formed with coordinated bonds between transition metal ions and organic ligands, which have rich nitrogen content, abundant

Electronic supplementary material The online version of this article (https://doi.org/10.1007/s00604-020-04531-0) contains supplementary material, which is available to authorized users.

✉ Wei Sun
sunwei@hainnu.edu.cn

[1] Key Laboratory of Laser Technology and Optoelectronic Functional Materials of Hainan Province, Key Laboratory of Functional Materials and Photoelectrochemistry of Haikou, College of Chemistry and Chemical Engineering, Hainan Normal University, Haikou 571158, People's Republic of China

[2] Key Laboratory of Optic-electric Sensing and Analytical Chemistry for Life Science of Ministry of Education, Shandong Key Laboratory of Biochemical Analysis, College of Chemistry and Molecular Engineering, Qingdao University of Science and Technology, Qingdao 266042, People's Republic of China

pore structure and large surface area [10]. Among them, ZIF-8 ($[Zn(2\text{-}mIm)_2]_n$, mIm is methylimidazole) and ZIF-67 ($[Co(2\text{-}mIm)_2]_n$) are known as two representative ZIFs, which have the same zeolite-like topological structure, alike unit lattice parameters, and identical organic ligand [11]. Since ZIF-67 and ZIF-8 are isostructural, a well-defined core-shell ZIF-8@ZIF-67 nanostructure can be created by epitaxial growth. Owing to the considerably abundant nitrogen contents, high conductivity, high metal ion contents, and low cost, core-shell ZIF@ZIF crystals have been proved as good candidate and excellent precursor materials to design a particular core-shell nanostructure [12, 13]. However, the porous carbon may be easily shelled with insufficient exposure of active sites under harsh conditions. Recently, the noble metal nanoparticles@porous carbons derived from MOFs nanocomposite have been reported for electrochemical applications because the loaded noble metal nanoparticles can keep their catalytic capacity when the small active molecules diffuse in and out of the porous carbon [14, 15]. For examples, Yang et al. prepared the hollow Zn/Co ZIFs derived from ZIF-67@ZIF-8 as the semi-hydrogenation of acetylene catalyst [12]. Yang et al. fabricated the gold nanoparticles @nitrogen-doped porous carbon derived from metal nanoparticles@ZIF-8 for hydrazine electrocatalysis [15]. Chen et al. [16] prepared the Pd nanoparticles stabilized with N-doped porous carbon that derived from ZIF-8 for selective catalysis in biofuel upgrade.

Herein, we constructed a novel nanocomposite of Au-Co bimetal nanoparticles embedded in nitrogen-doped carbon nanotube hollow polyhedron (NCNHP) through a pyrolysis-reduction method derived from core-shell ZIF-8@ZIF-67 (Scheme 1). The seed ZIF-8 derived nitrogen-doped carbon (Zn will disappear when the temperature exceeds 900 °C [17]) was acted as the structured hollow with ZIF-67 formed on the surface of ZIF-8 framework to promote the diffusion kinetics [11, 18, 19]. Also many carbon nanotubes could be produced on the surface of hollow polyhedron after the carbonization treatment of ZIF-8@ZIF-67. Electrochemical measurements displayed that Au-Co@NCNHP showed outstanding performance in electrooxidation and voltammetric determination of QR. The practical applications were realized by determination of QR contents in onion and drug samples with satisfactory results.

Experimental

Reagents and apparatus

Zinc nitrate hexahydrate, cobalt nitrate hexahydrate, 2-methylimidazole, absolute methanol (MeOH), and sodium borate ($NaBH_4$) were obtained from Shanghai Aladdin Chemical Reagent Company, China. Chloroauric acid ($HAuCl_4$) was purchased from Guangzhou Lixin Chemical Plant, China. 0.1 mol/L phosphate buffered solutions were used as supporting electrolyte with ultrapure water (Merck Millipore, Milli-Q IQ7000, France). All the reagents were of analytical grade and used as received.

X-ray diffraction (XRD) was carried out with a D2 phaser advance diffractometer with monochromatized Cu Kα radiation (λ = 1.5406 Å, Bruker, Germany). Scanning electron microscopy (SEM) was performed on a JSM-7100F electron microscope (JEOL, Japan). Transmission electron microscopy (TEM), high resolution transmission electron microscopy (HRTEM), and high-angle annular dark-field scanning transmission electron microscopy (HAADF-STEM) elemental mapping were operated by a JEM-2100F electron microscope (JEOL, Japan). X-ray photoelectron spectrum (XPS) was performed on an Escalab 250Xi spectrometer (Thermo Scientific, America). N_2 absorption-desorption isotherms were collected and calculated with Brunauer Emmett Teller-Barrett Joyner Halenda method (BET-BJH) and density functional theory (DFT). N_2 adsorption-desorption experiments were carried out at 77 K on an ASAP 2020 Model (Micromeritics, America). Fourier transform infrared (FT-IR) spectrum was observed with Nicolet 6700 FT-IR spectrometer (Thermo Fisher Scientific, America). Raman spectra were recorded on a LabRAM HR Evolution (Horiba Scientific, France). The

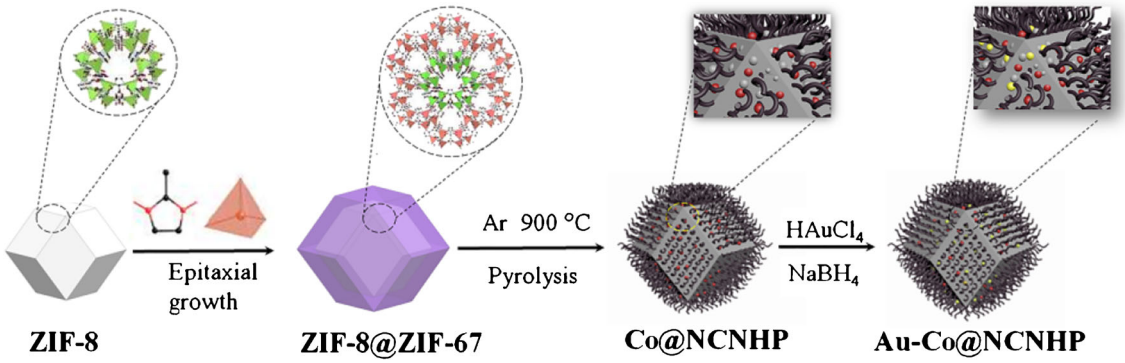

Scheme 1 Schematic illustration of the synthesis process of Au-Co@NCNHP

carbonization process was performed by a KMTF-1100 vacuum tube furnace (Anhui Kemi Equipment Technology, China). CHI 832B electrochemical workstation (Shanghai Chenhua Instrument, China) was applied for the electrochemical survey. A classical three-electrode system was obtained with a platinum wire as the counter electrode, Ag/AgCl (saturated KCl) as the reference electrode and the modified GCE ($\phi = 3$ mm) as the working electrode. HPLC analysis was performed with an Agilent 1200 (Agilent Technologies, America) equipped with a 50-μL automatic injection loop. Chromatographic separation was performed using Agilent Diamonsil C18 column (250 mm × 4.6 mm, 5 μm, America). HPLC mobile phase was consisted of a 0.2% phosphoric acid–methanol (40:60, v/v) mixture, which was filtered through a 0.45-μm filter, followed by degassing under vacuum and passed with the flow rate of 0.5 mL/min at injection volume of 10 μL. The detection process was carried out at the ambient temperature with the detector wavelength set at 368 nm.

Synthesis of Au-Co@NCNHP

The core-shell ZIF-8@ZIF-67 was synthesized according to previous literature with minor modification [20]. ZIF-8 crystals were prepared by the mixture of $Zn(NO_3)_2$ (0.01 mol, 75 mL) and 2-mIm (0.035 mol, 75 mL) in MeOH, which was used as seeds via vacuum drying after centrifuging and washing with MeOH for thrice. Then ZIF-67 shell was formed on the prepared ZIF-8 crystals. Firstly 2-mIm MeOH solution (0.02 mol, 100 mL) was added to disperse the seeds in MeOH solution with stirring for 10 min. Then $Co(NO_3)_2$ (0.02 mol, 100 mL) MeOH solution was mixed with the above solution, and the mixture was agitated for 24 h at ambient temperature. The light purple precipitates were collected by centrifugation, washed several times with MeOH, and dried in a vacuum oven at 70 °C for 6 h.

Co@NCNHP nanocomposites were prepared by direct pyrolyzation of ZIF-8@ZIF-67 at 900 °C with a stepping rate of 2 °C/min for 3 h under Ar atmosphere in a tube furnace. For preparing Au-Co@NCNHP, 40.0 mg Co@NCNHP was dispersed in 4.0 mL ethanol/water (1:1 in volume) solution, then 0.5 mL $HAuCl_4$ (1.3 mg/mL) solution was added under stirring and kept stirring for 4 h. Finally, the mixture was mixed with 4.0 mL $NaBH_4$ (0.05 mol/L) solution, and the resultant black precipitate was centrifuged and washed by ethanol.

Fabrication of the modified electrode

Before modification, GCE was prepolished with Al_2O_3 powder (0.05 μm), then washed thoroughly with water, ethanol, and water with the aid of ultrasonication, respectively. Then 8.0 μL Au-Co@NCNHP homogeneous suspension (1.0 mg/mL) was coated onto the surface of GCE and dried overnight. For comparison, Co@NCNHP/GCE and ZIF-8@ZIF-67/GCE were prepared by the similar procedures.

Electrochemical measurements

Electrochemical impedance spectroscopy (EIS) was conducted with a 10.0 mmol/L $[Fe(CN)_6]^{3-/4-}$ and 0.1 mol/L KCl mixture solution. Electrochemical properties of different electrodes were investigated by cyclic voltammetry (CV). The determinations of analyte were investigated by differential pulse voltammetry (DPV) in 0.1 mol/L phosphate buffered solution (pH 2.0) within the range from -0.2 to 0.8 V.

Samples analysis

Onions were purchased from a local vegetable market and dealt with the following procedure. Firstly, onions were cut up absolutely, and 5.0 g of the resultant paste was dissolved in 50 mL ethanol under sonication for 40 min. Then the solution was centrifuged at 4000 rpm for 10 min. Finally, 1.0 mL of the supernatant liquid was attenuated to 9.0 mL with 0.1 mol/L phosphate buffered solution (pH 2.0) for electrochemical detection.

Ginkgo tablets were purchased from a pharmacy (Haikou Qili Pharmaceutical Co. Ltd., China, Z20053069) and treated by following process. Two ginkgo tablets were grinded entirely, and the resultant powder was dissolved in 10 mL ethanol under sonication for 30 min. Then the mixture liquid was filtrated and further diluted to 50 mL with ethanol, and used as medical sample.

Results and discussion

Characterization of Au-Co@NCNHP

Scheme 1 reveals the preparation process of Au-Co@NCNHP nanocomposites. SEM and TEM images (Fig. S1) illustrate that ZIF-8 and ZIF-8@ZIF-67 display well-defined rhombic dodecahedral shape with smooth surfaces and uniformly dispersed size. After carbonization, Co@NCNHP shows hollow polyhedron shape with coarse surface settled with plenty carbon nanotubes (Fig. S2A–D). During this carbonization process, the released gas helps Zn^{2+} to move out, and promotes the formation of hollow polyhedron. After subsequent reduction of $HAuCl_4$ in boric acid, Au nanoparticles are formed on the surface of Co@NCNHP to get Au-Co@NCNHP. SEM (Fig. 1a, Fig. S2E and 2F) and TEM (Fig. 1c–e) images show that the hollow polyhedron made of carbon nanotube also keeps and displays high porosity. HAADF-STEM (Fig. 1b) and energy-dispersive X-ray spectroscopy (EDS) elemental mapping images (Fig. 1g) illustrate that C, N, Co, and Au elements are evenly distributed over the entire NCNHP. The

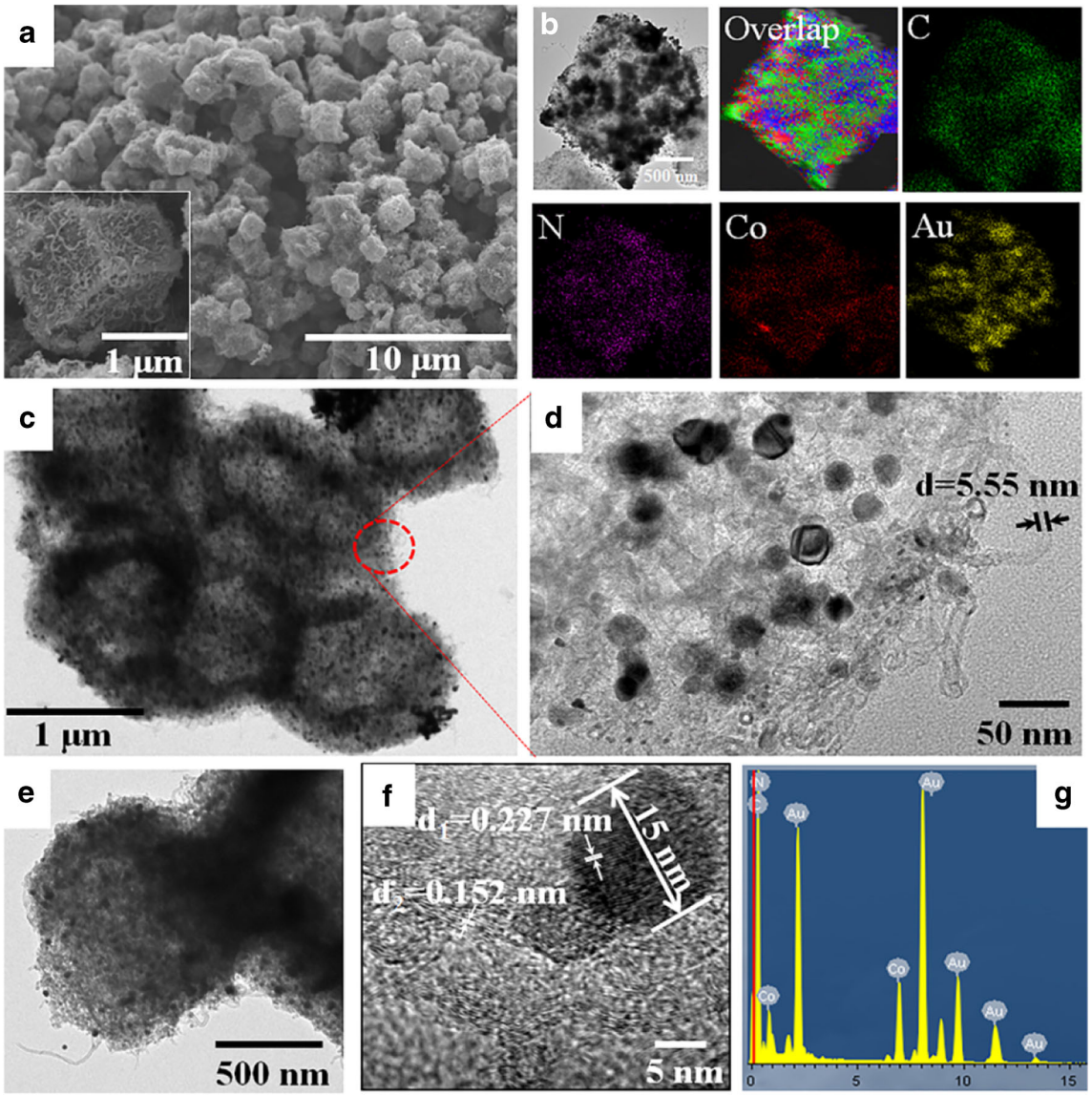

Fig. 1 **a** SEM, the inset was the magnified image; **b** HAADF-STEM elemental mapping; **c** and **e** TEM; **d** and **f** HRTEM; **g** EDS of Au-Co@NCNHP

HRTEM images of Au-Co@NCNHP (Fig. 1d and f) display the average diameter of carbon nanotubes as 5.5 nm ($n = 10$) and the average diameter of nanoparticles as 15 nm ($n = 15$).

Figure 2a shows the XRD patterns of ZIF-8@ZIF-67, Co@NCNHP, and Au-Co@NCNHP, respectively. The characteristic peaks of ZIF-8 nearly match the literature results [21]. XRD pattern of Co@NCNHP reveals four peaks located at 25.9°, 44.1°, 51.4°, and 75.9°; indexes to (002) diffractions of graphitic carbon; and (111), (200), and (220) lattice planes of Co. XRD pattern of Au-Co@NCNHP shows the peaks at 38.2°, 44.4°, 64.6°, and 78.8°, corresponding to (111), (200), (220), and (311) facets of Au [22]. Furthermore, the structures of ZIF-8@ZIF-67, Co@NCNHP, and Au-Co@NCNHP were investigated by using Raman spectroscopy (Fig. 2b). Raman spectrum of ZIF-8@ZIF-67 displays four peaks located at 176, 465, 515, and 677 cm^{-1}, corresponding to characteristic lines of the Co(Zn)-N, Co-O-Co, Zn-O-Zn, and 2-mIm ring. The peaks of Co@NCNHP and Au-Co@NCNHP around 1314 cm^{-1} and 1584 cm^{-1} can be assign to D and G band, respectively [23]. Remarkably, the intensity ratio of these bands (I_D/I_G), which reflects the unordered carbon material, is 0.78 (Co@NCNHP) and 0.98 (Au-Co@NCNHP). These reveal a low graphitic crystallinity of Au-Co@NCNHP. Figure 2c presents the FT-IR spectra of the ZIF-8@ZIF-67 precursor and the as-prepared samples. Although the spectra of each NCNHP are complicated, the samples of Co@NCNHP and Au-Co@NCNHP show a similar FT-IR spectrum. As listed in Table S1, all these peaks are assigned to the usual functional groups of materials.

The composition of as-prepared nanocomposites was recorded by XPS, as shown in Fig. 2d. Full surveys of ZIF-8@ZIF-67, Co@NCNHP, and Au-Co@NCNHP

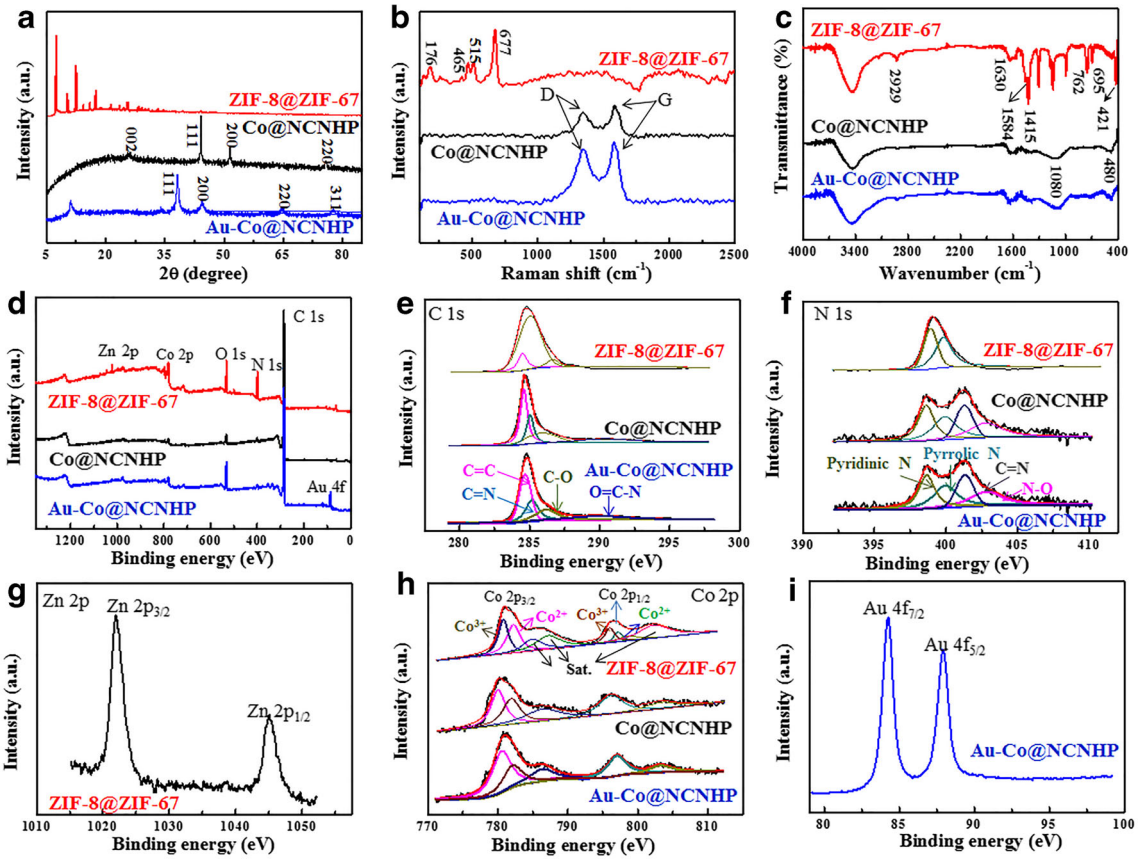

Fig. 2 **a** XRD pattern; **b** Raman spectra; **c** FT-IR spectra; **d** survey XPS spectra; **e** C 1s; **f** N 1s; **g** Zn 2p; **h** Co 2p, and **i** Au 4f fitting of samples

involve C 1s, N 1s, O 1s, Co 2p, Zn 2p, and Au 4f peaks. The pyrolyzation of ZIF-67@ZIF-67 to Co@NCNHP can be mainly confirm by the presence of C1s peak (Fig. 2e), which have four carbon atomic components including C=C (284.6 ± 0.2 eV), C=N (285.2 ± 0.2 eV), C-O (285.8 ± 0.2 eV), and O=C-N (288.1 ± 0.2 eV), which has a considerable decrease in the degree of carbonization compared with the ZIF-67@ZIF-67 precursor [24]. The C 1s peak mainly assigns to the C=C, indicating the efficient carbonization of ZIF-67@ZIF-67. The chemical states of N and Co in the sample were also examined. After carbonization, four N-types including N-O (402.8 ± 0.2 eV), C=N (401.0 ± 0.2 eV), pyrrolic (400.0 ± 0.2 eV), and pyridinic (398.4 ± 0.2 eV) can be distinguished from N 1s spectrum (Fig. 2F) [25]. Furthermore, no signal peak can be found from the Zn 2p spectrum of Co@NCNHP and Au-Co@NCNHP (Fig. 2g), which display that Zn element had been evaporated absolutely. For the high-resolution spectrum of Co 2p (Fig. 2h), two major peaks with binding energies at 797.3 ± 0.2 eV and 780.3 ± 0.2 eV are characteristics of Co $2p_{1/2}$ and Co $2p_{3/2}$, respectively [26]. As shown in Fig. 2i, the Au 4f spectrum is contained a doublet at binding energy of 84.0 eV and 87.6 eV, which are assigned to Au $4f_{7/2}$ and $4f_{5/2}$ lines, respectively. These values are clearly indicated that Au nanoparticles are still in metallic form.

The surface area of Au-Co@NCNHP (Fig. 3a, Table S2) is much smaller than that of ZIF-8@ZIF-67 (Fig. S3A and S3B), attributing to the dismounting of the well-defined micropores. Pore size distributions of Co@NCNHP and Au-Co@NCNHP exhibit type IV isotherm, showing the presence of both micropores and mesopores (Fig. 3b, S3C and S3D). The presence of porous structure can allow electrolyte to reach the active sites and simultaneously improve the catalytic efficiency [27].

Electrochemical investigations

The effective surface area (A) of the electrode can be calculated by the Randles-Sevcik expression $[I_p = (2.69 \times 10^5) n^{3/2} A D^{1/2} C_0 \upsilon^{1/2}]$ with the slope of I_p vs. $\upsilon^{1/2}$. As for Au-Co@NCNHP/GCE, the A value was found as 0.194 cm^2, which was 1.4 times larger than that of bare GCE (0.134 cm^2). Therefore, the increase of the effective surface area using Au-Co@NCNHP is attributed to the porous structure of NCNHP, the high conductivity of bimetal structure, and their synergistic effects in facilitating the diffusional process of $[Fe(CN)_6]^{3-/4-}$ through the channel formed on the electrode surface.

Electrochemical behaviors of 100.0 μmol/L QR on different electrodes were studied by CV in pH 2.0 phosphate buffered

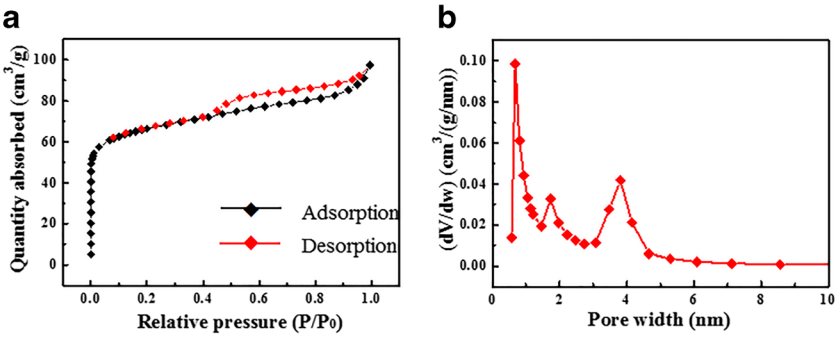

Fig. 3 N_2 adsorption-desorption isotherm **a** and pore size distribution curves **b** of Au-Co@NCNHP

solution at the scan rate of 0.1 V/s. On GCE (Fig. 4a, curve a) and ZIF-8@ZIF-67/GCE (Fig. 4a, curve b), the redox peaks are smaller. On Co@NCNHP/GCE (Fig. 4a, curve c) two anodic peaks occur at the potentials of 0.47 V (A1) and 0.59 V (A2), which are assigned with oxidation of the two hydroxyl groups of QR. Two cathodic peaks at 0.44 V (C1) and 0.57 V (C2) corresponding to reduction of the oxidation products can also be observed [28]. On Au-Co@NCNHP/GCE, biggest redox peaks can be found (Fig. 4a, curve d), which display that Au nanoparticles and Co@NCNHP have synergistic effects in QR electrochemical reaction. Au nanoparticles have excellent conductivity with catalytic activity, and Co@NCNHP has large active sites with high porosity. Therefore the combination of Au nanoparticles and Co@NCNHP lead to the changes of the electronic structure with the electron transfer rate enhanced, and the resulted sensitive current responses [22].

The solution pH has strong effect on the electrochemical behavior of QR on the Au-Co@NCNHP/GCE, which was studied at the scan rate of 0.1 V/s. As seen from Fig. 4b, two oxidation peaks (A1 and A2) appear, which are due to the electrooxidation of QR molecules, and the o-quinone is easily formed at lower pH range of phosphate buffered solution (1~4). But excessively higher pH (5~8) is disadvantageous to the formation of o-quinone and the electron transfer can be hampered. The oxidation peak (A1) potentials (E_{pa1}) are shifted negatively with the increase of pH, indicating that protons participate in electrochemical reaction. The oxidation peak currents (I_{pa1}) of QR are increased with the pH value

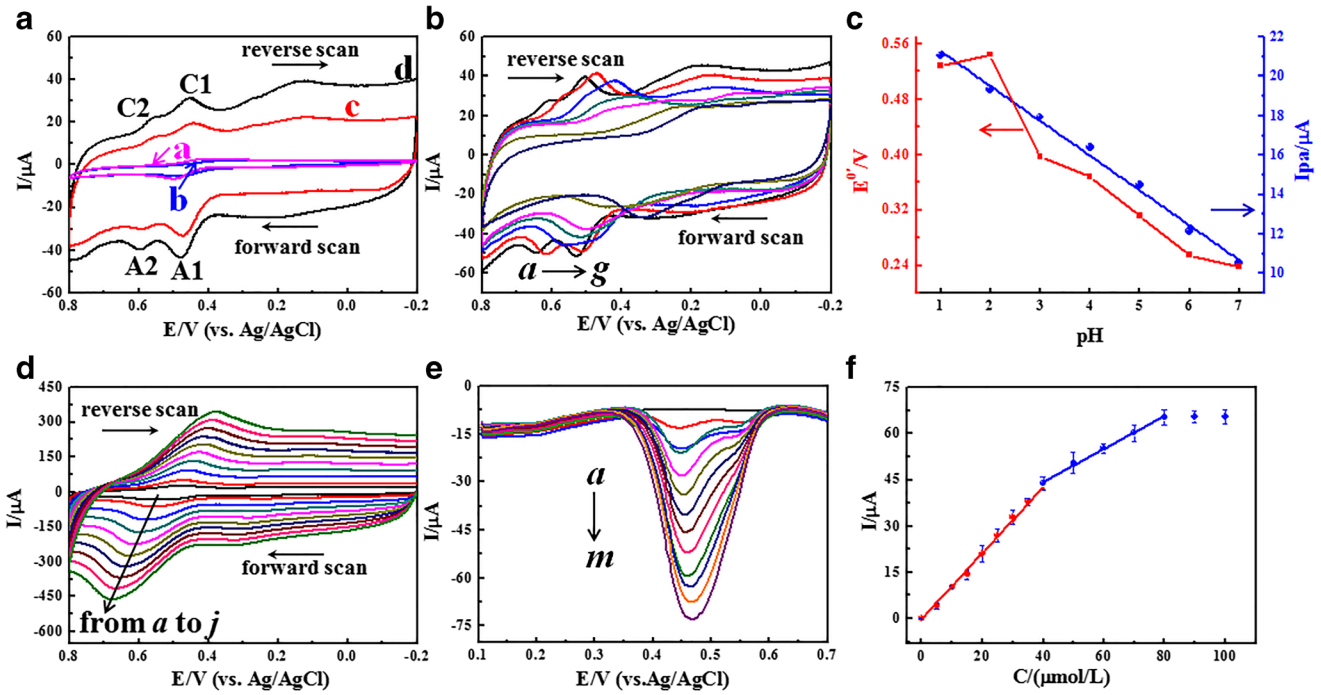

Fig. 4 **a** CV of 100.0 μmol/L QR on GCE (a), ZIF-8@ZIF-67/GCE (b), Co@NCNHP/GCE (c) and Au-Co@NCNHP/GCE (d) in pH 2.0 phosphate buffered solutions at the scan rate of 0.1 V/s; **b** CV of 100.0 μmol/L QR on Au-Co@NCNHP/GCE with different pH phosphate buffered solutions (a-g: 1, 2, 3, 4, 5, 6, 7) at the scan rate of 0.1 V/s; **c** Relationships of $E^{0\prime}$ and I_{pa} with pH; **d** CV of 100.0 μmol/L QR on Au-Co@NCNHP/GCE at different scan rates in pH 2.0 phosphate buffered solutions (a–j: 0.05, 0.1, 0.2, 0.3, 0.4, 0.5, 0.6, 0.7, 0.8, 0.9 V/s); **e** DPV curves of QR with different concentrations in pH 2.0 phosphate buffered solutions (a–m: 0.05, 5.0, 10.0, 15.0, 20.0, 25.0, 30.0, 35.0, 40.0, 50.0, 60.0, 70.0, and 80.0 μmol/L); **f** The relation between I_{pa} and QR concentration

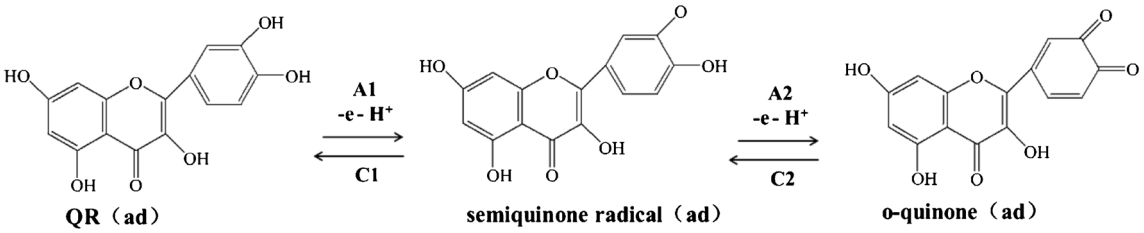

Scheme 2 Consecutive electrooxidation mechanism of QR

from 1.0 to 2.0, and then decreased as the further increasing of pH (Fig. 4c). At pH 2.0 the largest I_{pa1} value appears, which is selected as the optimum buffer pH with enough protons provided. The linear regression equation of $E^{0'}$ with pH is achieved as $E^{0'}$ (V) = (0.599 ± 0.006)–(0.050 ± 0.001) pH. The slope value (50 mV/pH) is close to 59 mV/pH, illustrating an equal proton-electron transfer electrode process [29].

As observed from Fig. 4d, the effect of different scan rates (50 to 900 mV/s) on the peak (A1 and C1) current of 100.0 μmol/L QR was investigated in phosphate buffered solution (pH 2.0) at Au-Co@NCNHP/GCE. The redox peak currents are increased linearly with the square root of scan rate ($\nu^{1/2}$), and the equations are expressed as I_{pa} (μA) = (− 269.2 ± 8.9) $\nu^{1/2}$ $(V/s)^{1/2}$ + (53.6 ± 4.2) and I_{pc} (μA) = (139.3 ± 4.5) $\nu^{1/2}$ $(V/s)^{1/2}$–(15.6 ± 2.2) (Fig. S4A). These results show that electrochemical process of QR is predominantly diffusion-controlled process [30]. At the same time, the anodic/cathodic peak potential (E_{pa}/E_{pc}) shift positively/negatively with increasing scan rate. As shown in Fig. S4B, E_p and ln ν have linear relationships as E_{pa1} (V) = (0.0728 ± 0.0026) ln ν + (0.682 ± 0.002) and E_{pc1} (V) = (− 0.0561 ± 0.0015) ln ν + (0.372 ± 0.001), respectively. From Laviron's equation [31], electrochemical parameters were calculated with electron transfer number (n) as 1.22, electron transfer coefficient (α) as 0.56, and heterogeneous electron transfer rate constant (k_s) as 0.89 s^{-1}. The k_s data is larger than some reported values such as on multiwalled carbon nanotube-paraffin oil paste electrode (0.546 s^{-1}) [29], graphene modified electrode (5.19×10^{-6} s^{-1}) [32] and gold nanoparticles-graphene modified electrode (0.25 s^{-1}) [33], illustrating a faster transfer rate with Au-Co@NCNHP as the modifier and the enhancer. Therefore the high conductive Au-Co bimetal decorated NCNHP can provide a fast electron transfer interface for QR to take place the reaction. The possible consecutive electrooxidation mechanism of QR could be expressed in Scheme 2.

Figure 4e shows the DPV curves for the analysis of standard QR solutions under optimized conditions. At low QR concentrations, small changes in concentration can cause significant changes in current response due to the presence of diffusion effects. Furthermore, QR can be rapidly depleted as substrate to convert into o-quinone at the local concentration of the electrode surface. At high QR level, the electrode surface may be saturated with large changes in concentration caused small changes in current responses [7, 34, 35]. The dependence of I_{pa} on QR concentration is plotted from 0.050 to 35.00 μmol/L with the linear regression equation of I_{pa} (μA) = (1.066 ± 0.023) C (μmol/L) + (0.027 ± 0.003) (Fig. 4F). The limit of detection is 0.023 ± 0.002 μmol/L (3σ). From the calibration curve, the sensitivity is obtained as 5.49 μA·(μmol/L)$^{-1}$·cm^{-2}. Compared with other different modified electrodes for QR analysis, the resultant Au-Co@NCNHP/GCE presents higher sensitivity and wider linear range (Table S3).

Anti-interference, reproducibility, and stability

In order to assess the anti-interferences of Au-Co@NCNHP/GCE toward the QR analysis, we investigated the electrochemical behaviors of different potentially interfering compounds such as glucose (0.1 mmol/L), glycine (0.1 mmol/L), citric acid (0.1 mmol/L), ascorbic acid (0.1 mmol/L), uric acid (0.1 mmol/L), dopamine (0.05 mmol/L), rutin (0.01 mmol/L), lutcolin (0.01 mmol/L), baicalin (0.01 mmol/L), KCl (1.0 mmol/L), $CoCl_2$ (1.0 mmol/L), and $NaNO_3$ (1.0 mmol/L) with 10.0 μmol/L QR. It can be observed that the current peaks of QR are not obviously altered, which indicates that this sensor possesses good anti-interferences

Table 1 Determination results of QR in real samples (n = 3)

Sample	Detected (μmol/L)	Added (μmol/L)	Total (μmol/L)	Recovery (%)	RSD (%)
Onions	1.03	2.50	3.54	100.3	2.68
		5.00	6.18	102.5	3.52
		10.00	10.89	98.73	1.73
Ginkgo tablets	13.11	5.00	17.74	97.96	1.23
		10.00	23.28	100.7	3.25
		15.00	28.65	101.9	2.79

ability (Table S4). The repeatability of this sensor was measured by 10.0 μmol/L QR with six Au-Co@NCNHP/GCEs fabricated independently. The relative standard deviation (RSD) of ten times successive detection with RSD of the same electrode is 2.8%, and six Au-Co@NCNHP/GCE is 6.4%. The results illustrate that the modified electrode has good reproducibility. The modified electrode is stored in refrigerator at 4 °C, and after 7 days storage the response current to 10.0 μmol/L QR are retained 97.2% of its original value with RSD as 3.8%, which reflects the good stability of Au-Co@NCNHP/GCE.

Samples detection

In order to evaluate the practical utility of the present method, onions and drug samples were analyzed by using Au-Co@NCNHP/GCE via DPV. Onions are ranked highest in QR content in a survey of 28 vegetables and 9 fruits [36, 37]. The amount of QR in onions varies depending on bulb color and type, which is distributed mostly in the outer skin and rings [38]. The QR contents in onions and ginkgo tablets were determined, and the results are summarized in Table 1, which showed satisfactory data and recovery value. Also, a reported HPLC procedure for the QR analysis in onions samples was performed according to the reference [39], which gave the value of 1.13 ± 0.05 μmol/L. The result is closely agreement with the electrochemical data, indicating the practical application of this modified electrode.

Conclusion

In this paper, a novel sensing platform for QR was fabricated based on an Au-Co@NCNHP nanocomposite modified GCE. Core-shell ZIF-8@ZIF-67 was synthesized by colloidal chemical procedure, which was carbonized to get a Co@NCNHP with shape of carbon nanotube hollow polyhedron. Then Au nanoparticles were further formed on surface and core of Co@NCNHP by reduction of boric acid to obtain an Au-Co bimetal decorated NCNHP (Au-Co@NCNHP). Because NCNHP had large specific surface and high porosity, and Au-Co bimetal had high conductivity with strong electrocatalysis, the composite exhibited synergistic effects including large specific surface area, and high electrochemical activity toward QR. However, flavonoids compound with similar structures may lead to the interference due to the close peak potential. The ginkgo tablet and onions samples were detected successfully, which displayed the practical applications of the sensor by using Au-Co@NCNHP/GCE.

Funding This project was financially supported by the National Natural Science Foundation of China (21665007, 21964007), the National College Students Innovation and Entrepreneurship Training Program (30101100307), Graduate Student Innovation Research Projects of Hainan Normal University (Hsyx2018-9), Hainan Provincial Natural Science Foundation of High Level-talent Project (2019RC188), and Open Project of Chemistry Department of Qingdao University of Science and Technology (QUSTHX201935).

Compliance with ethical standards

Conflict of interest The authors declare that they have no conflict of interest.

Ethical approval All the experiments were performed in compliance with the ethical standards of the relevant laws and institutional guideline of P. R. China, and with the 1964 Helsinki declaration. The studies were approved by the Ethics Committee of the College of Chemistry and Chemical Engineering, Hainan Normal University, P. R. China.

References

1. Gomez FJV, Espino M, Fernandez MDLA, Raba J, Silva MF (2016) Enhanced electrochemical detection of quercetin by natural deep eutectic solvents. Anal Chim Acta 936:91–96
2. Ghoreishi SM, Masoum S, Mosleh M, Khoobi A (2018) Determination of quercetin in the presence of tannic acid in soft drinks based on carbon nanotubes modified electrode using chemometric approaches. Sensors Actuators B Chem 272:605–611
3. Xu B, Yang L, Zhao F, Zeng B (2017) A novel electrochemical quercetin sensor based on Pd/MoS_2-ionic liquid functionalized ordered mesoporous carbon. Electrochim Acta 247:657–665
4. Jones DJL, Lim CK, Ferry DR, Gescher A (2015) Determination of quercetin in human plasma by HPLC with spectrophotometric or electrochemical detection. Biomed Chromatogr 12:232–235
5. Wu D, Chen Z (2014) ZnS quantum dots-based fluorescence spectroscopic technique for the detection of quercetin. Luminescence 29:307–313
6. Nielsen SE, Dragsted LO (1998) Column-switching high-performance liquid chromatographic assay for the determination of quercetin in human urine with ultraviolet absorbance detection. J Chromatogr B Biomed Sci Appl 707:81–89
7. Zhang W, Zong L, Geng G, Li Y, Zhang Y (2018) Enhancing determination of quercetin in honey samples through electrochemical sensors based on highly porous polypyrrole coupled with nanohybrid modified GCE. Sensors Actuators B Chem 257: 1099–1109
8. Sun S, Zhang M, Li Y, He X(2013) A molecularly imprinted polymer with incorporated graphene oxide for electrochemical determination of quercetin. Sensors 13:5493–5506
9. Niu X, Li X, Chen W, Li X, Weng W, Yin C, Dong R, Sun W, Li G (2018) Three-dimensional reduced graphene oxide aerogel modified electrode for the sensitive quercetin sensing and its application. Mater Sci Eng C 89:230–236
10. Kyo Sung P, Zheng N, Cote AP, Jae Yong C, Rudan H, Uribe-Romo FJ, Chae HK, Michael OK, Yaghi OM (2006) Exceptional chemical and thermal stability of zeolitic imidazolate frameworks. Proc Natl Acad Sci U S A 103:10186–10191
11. Jing T, Salunkhe RR, Jian L, Torad NL, Masataka I, Shuhei F, Yusuke Y (2015) Thermal conversion of core-shell metal-organic frameworks: a new method for selectively functionalized nanoporous hybrid carbon. J Am Chem Soc 137:1572–1580
12. Yang J, Zhang F, Lu H, Hong X, Jiang H, Wu Y, Li Y(2015) Hollow Zn/Co ZIF particles derived from core-shell ZIF-

67@ZIF-8 as selective catalyst for the semi-hydrogenation of acetylene. Angew Chem 127:11039–11043
13. Rosler C, Aijaz A, Turner S, Filippousi M, Shahabi A, Xia W, Van TG, Muhler M, Fischer RA (2016) Hollow Zn/Co zeolitic imidazolate framework (ZIF) and yolk-shell metal@Zn/Co ZIF nanostructures. Chemistry 22:3304–3311
14. Xin G, Li L, Zhang X, Chen J (2015) Platinum nanoparticles encapsulated in nitrogen-doped mesoporous carbons as methanol-tolerant oxygen reduction electrocatalysts. Chemelectrochem 2: 404–411
15. Yang J, Zhao F, Zeng BZ (2016) Well-defined gold nanoparticle@N-doped porous carbon prepared from metal nanoparticle@metal-organic frameworks for electrochemical sensing of hydrazine. RSC Adv 6:23403–23410
16. Chen YZ, Cai GR, Wang YM, Qiang X, Yu SH, Jiang HL (2016) Palladium nanoparticles stabilized with N-doped porous carbons derived from metal-organic frameworks for selective catalysis in biofuel upgrade: the role of catalyst wettability. Green Chem 18: 1212–1217
17. Yin P, Yao T, Wu Y, Zheng L, Lin Y, Liu W, Ju H, Zhu J, Hong X, Deng Z (2016) Single cobalt atoms with precise N-coordination as superior oxygen reduction reaction catalysts. Angew Chem 128: 10958–10963
18. Chen YZ, Wang C, Wu ZY, Xiong Y, Xu Q, Yu SH, Jiang HL (2015) From bimetallic metal-organic framework to porous carbon: high surface area and multicomponent active dopants for excellent electrocatalysis. Adv Mater 27:5010–5016
19. Liu S, Wang Z, Zhou S, Yu F, Yu M, Chiang CY, Zhou W, Zhao J, Qiu J (2017) Metal-organic-framework-derived hybrid carbon nanocages as a bifunctional electrocatalyst for oxygen reduction and evolution. Adv Mater 29:1700874
20. Zhang J, Zhang T, Xiao K, Cheng S, Feng Y (2016) A novel and facile strategy for controllable synthesis of multi-layered core-shell zeolitic imidazolate frameworks. Cryst Growth Des 16:6494–6498
21. Pan Y, Sun K, Liu S, Cao X, Wu K, Cheong WC, Chen Z, Wang Y, Li Y, Liu Y (2018) Core-shell ZIF-8@ZIF-67 derived CoP nanoparticles-embedded N-doped carbon nanotube hollow polyhedron for efficient over-all water splitting. J Am Chem Soc 140: 2610–2618
22. Huang SS, Liu L, Mei LP, Zhou JY, Guo FY, Wang AJ, Feng JJ (2015) Electrochemical sensor for nitrite using a glassy carbon electrode modified with gold-copper nanochain networks. Microchim Acta 183:791–797
23. Hsin YL, Hwang KC, Yeh C-T (2007) Poly (vinylpyrrolidone)-modified graphite carbon nanofibers as promising supports for PtRu catalysts in direct methanol fuel cells. J Am Chem Soc 129: 9999–10010
24. Shi X, Zhang Z, Yun F, Gan Y (2015) Self-template synthesis of nitrogen-doped porous carbon derived from zeolitic imidazolate framework-8 as an anode for sodium ion batteries. Mater Lett 161:332–335
25. Cao F, Zhao M, Yu Y, Chen B, Huang Y, Yang J, Cao X, Lu Q, Zhang X, Zhang Z, Tan C, Zhang H (2016) Synthesis of two-dimensional $CoS_{1.097}$/nitrogen-doped carbon nanocomposites using metal-organic framework nanosheets as precursors for supercapacitor application. J Am Chem Soc 138:6924–6927
26. Liu S, Wang J, Wang J, Zhang F, Liang F, Wang L (2014) Controlled construction of hierarchical $Co_{1-x}S$ structures as high performance anode materials for lithium ion batteries. CrystEngComm 16:814–819
27. Mao C, Kong A, Wang Y, Bu X, Feng P (2015) MIL-100 derived nitrogen-embodied carbon shells embedded with iron nanoparticles. Nanoscale 7:10817–10822
28. Maria A, Brett O, Ghica ME (2003) Electrochemical oxidation of quercetin. Electroanalysis 15:1745–1750
29. Ping X, Zhao F, Zeng B (2007) Voltammetric determination of quercetin at a multi-walled carbon nanotubes paste electrode. Microchem J 85:244–249
30. Kissinger P, Heineman WR (1996) Laboratory techniques in electroanalytical chemistry, 2nd edn. Marcel Dekker, New York
31. Laviron E (1979) General expression of the linear potential sweep voltammogram in the case of diffusionless electrochemical systems. J Electroanal Chem 101:19–28
32. Arvand M, Anvari M (2013) A graphene-based electrochemical sensor for sensitive detection of quercetin in foods. J Iran Chem Soc 10:841–849
33. Zhu W, Chen T, Ma X, Ma H, Chen S (2013) Highly sensitive and selective detection of dopamine based on hollow gold nanoparticles-graphene nanocomposite modified electrode. Colloids Surf B: Biointerfaces 111:321–326
34. Gholizadeh A, Shahrokhian S, Iraji zad A, Mohajerzadeh S, Vosoughi M, Darbari S, Koohsorkhi J, Mehran M (2012) Fabrication of sensitive glutamate biosensor based on vertically aligned CNT nanoelectrode array and investigating the effect of CNTs density on the electrode performance. Anal Chem 84: 5932–5938
35. Yang C, Dong XX, Sun YM, Xu ZL, Li MY, Feng NN (2015) Nanoporous MgO based nonenzymatic electrochemical sensor for rapid screening of hydrogen peroxide in milk. RSC Adv 5:86485–86489
36. Slimestad R, Fossen T, Vagen IM (2007) Onions: a source of unique dietary flavonoids. J Agric Food Chem 55:10067–10080
37. Hertog MG, Hollman PC, Katan MB (1992) Content of potentially anticarcinogenic flavonoids of 28 vegetables and 9 fruits commonly consumed in the Netherlands. J Agric Food Chem 40:2379–2383
38. Zielinska D, Nagels L, Piskula M (2008) Determination of quercetin and its glucosides in onion by electrochemical methods. Anal Chim Acta 617:22–31
39. Nile SH, Nile AS, Keum YS, Sharmab K (2017) Utilization of quercetin and quercetin glycosides from onion (Allium cepa L.) solid waste as an antioxidant, urease and xanthine oxidase inhibitors. Food Chem 235:119–126